Robust Cardiac Rate Estimation of an Individual

Inoh Choi, Min Kim, Jaeho Choi, Jeongki Park, Sanghong Park, and Kyungtae Kim, *Member, IEEE*

***Abstract*—Impulse-radio ultra-wideband (IR-UWB) radar devices can be used to monitor vital signs, such as respiratory and cardiac rates. For this purpose, the phase of an echo signal received from the chest or back of a human is usually used; subsequently, respiratory rate estimation (RRE) and cardiac rate estimation (CRE) can be achieved by estimating two fundamental frequencies corresponding to the respiratory and cardiac rates, respectively. However, the interference caused by undesirable terms would inevitably be induced in an echo signal; thus, the cardiac rate information contained in the phase of the received signal is often smeared and destroyed. Among several sources of interference such as high-order harmonics of respiratory rate, random body movement of an individual, and system noise, the body movement of an individual is the most critical for reliable CRE, making it a very challenging task. To address this problem, we herein propose a new framework comprising four steps: 1) RRE via differentiation and spectrum analysis for an unwrapped phase of received signal, 2) coarse estimation of cardiac rate candidates, 3) selection of three promising candidates for the desired cardiac rate based on a histogram of several candidates, and 4) determination of the desired cardiac rate via a fuzzy logic rule-based method. In experiments using 7.29 GHz IR-UWB radar hardware, we observed that our proposed framework is capable of performing accurate and robust real-time CRE even in the presence of body movement.**

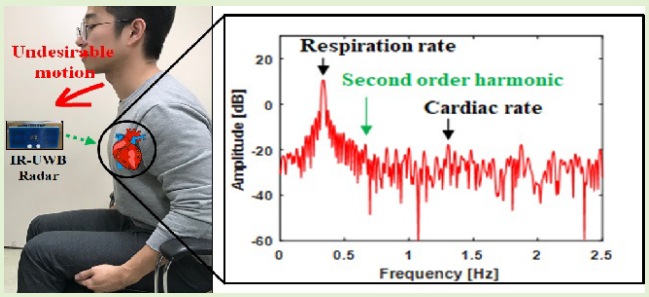

***Index Terms*—Vital sign estimation, phase sensing, phase interference, cardiac rate candidate, fuzzy logic-based method.**

I. Introduction

NONCONTACT vital sign (i.e., respiratory and cardiac rate) estimation (VSE) techniques based on radar systems have various applications in medical, leisure, and military fields [1]–[14]. Generally, VSE can be achieved by estimating very small-range variations caused by micromotions in an individual's body skin caused by vital signs. For this purpose, the phase information is extracted by applying arctangent demodulation [9] to a complex echo signal received from the chest or back of the individual, and the desired vital sign can be obtained by analyzing the phase; two fundamental frequencies correspond to the respiratory and cardiac rates [15]. For a more accurate VSE, phase sensing must be carried out based on a very high resolution, leading to a shorter wavelength (i.e., higher carrier frequency) [16]. However, the dynamic range for phase sensing is restricted to within a half-wavelength owing to the phase ambiguity, thus, the phase-unwrapping step in [17]–[18] is inevitable for reliable VSE. However, undesirable interference components such as high-order harmonics of respiratory rate, random body movement of an individual, and system noise usually exist in the measured and unwrapped phases. This makes VSE very challenging. Consequently, the mitigation of undesirable interferences included in the measured phase is a crucial step for robust and accurate VSE performance.

Several studies have been carried out on the VSE using radar carrier frequencies around 4–24 GHz [19]–[27]. Recently, a respiratory rate estimation (RRE) method under simple body movement (e.g., walking motion of an individual along the radial direction) using a single continuous-wave (CW) Doppler radar sensor was proposed [19]. However, in [19], the corruption of phase information due to this body movement leads to a very low signal-to-noise ratio (SNR), thus, preventing robust cardiac rate estimation (CRE). To solve this problem, Li and Jin [20] proposed a method of canceling signals from body movement using two echo signals received from both the chest and the back. However, unlike chest measurements, back measurements are less likely to faithfully reflect skin vibrations directly linked to cardiac activity, leading to a substantial degradation of performance in signal cancellation. For more accurate back measurements, Schires *et al.* [21] presented a strategy using an impulse-radio ultra-wideband

Manuscript received February 21, 2021; revised March 22, 2021; accepted April 17, 2021. Date of publication April 20, 2021; date of current version June 30, 2021. The associate editor coordinating the review of this article and approving it for publication was Dr. Ying Zhang. *(Corresponding author: Kyungtae Kim.)*

Inoh Choi is with the Department of Electronics and Communications Engineering, Korea Maritime & Ocean University, Busan 49112, South Korea (e-mail: inohchoi@kmou.ac.kr).

Min Kim, Jaeho Choi, Jeongki Park, and Kyungtae Kim are with the Department of Electrical Engineering, Pohang University of Science and Technology, Pohang 37673, South Korea (e-mail: skymeen@postech.ac.kr; jhchoi93@postech.ac.kr; pjkeee1@postech.ac.kr; kkt@postech.ac.kr).

Sanghong Park is with the Department of Electronic Engineering, Pukyong National University, Busan 48513, South Korea (e-mail: radar@pknu.ac.kr).

Digital Object Identifier 10.1109/JSEN.2021.3074510

(IR-UWB) radar sensor with a body-coupled antenna in the backrest of a car seat. However, when the body-coupled antenna is often disconnected from the back by an unexpected body movement of an individual, this strategy fails to perform the signal cancellation step.

On the contrary, Liu *et al.* [22] utilized an interferometer radar system based on the frequency-sweeping technique for accurate CRE, leading to improved dynamic range and robustness to system noise and standing waves. In addition, Gu *et al.* [23] and Yavari and Boric-Lubecke [24] proposed a digital postdistortion and compensation method to reduce the effect of undesirable interferences. In particular, as the phase of an echo signal received from an individual is approximately composed of a linear mixture of phase components corresponding to respiratory activity, cardiac activity, random body movement, among others, sophisticated signal decomposition approaches such as wavelet transform [25], empirical mode decomposition (EMD) [26], and variational mode decomposition (VMD) [27] have been exploited to improve the SNR for robust CRE.

In the conventional approaches discussed above, the cardiac rate is usually determined as a fundamental frequency corresponding to the maximum peak in the spectrum, except for the one corresponding to the respiratory rate. However, the existing methods [19]–[27] would no longer guarantee robust CRE performance because the amplitude of the cardiac rate in the spectrum obtained from the phase is occasionally much lower than that of strong phase noise caused by critical random body movement in a real-time CRE environment. Therefore, an additional strategy for obtaining the proper fundamental frequency originating from only cardiac vibrations is required to complete the real-time CRE in a practical situation. However, to the best of our knowledge, there has been no research on this topic.

The main contribution of this paper involves suggesting a new framework for robust and accurate real-time CRE, which is mainly composed of four steps: 1) RRE via differentiation and spectrum analysis for an unwrapped phase of received echoes, 2) coarse estimation of cardiac rate candidates by excluding the respiratory rate and its high-order harmonics, 3) selection of three promising candidates for the desired cardiac rate based on the frequencies that appear most often in the histogram, and 4) determination of the desired cardiac rate from the three promising ones via a fuzzy logic rule-based method.

Let us assume that the unwrapped phase of an echo signal received from an individual is approximately composed of a linear mixture of five phase components corresponding to respiratory activity, cardiac activity, random body movement, system noise, and background clutter. For RRE, the differentiation of phase is followed by a phase-unwrapping step in [17]–[18] to remove the frequency of direct current (DC) around zero originating from background clutter. RRE is relatively straightforward because it usually coincides with the fundamental frequency corresponding to the maximum peak in the spectrum obtained from an unwrapped and differentiated phase [15]. However, unlike RRE, CRE determination is extremely challenging in the presence of both the remaining high-order harmonics of the respiratory rate and the random movement of an individual. Fortunately, once the respiratory rate is obtained a *priori* via the above RRE process, its high-order harmonics can be easily predicted as integer multiples of the estimated respiratory rate. Nevertheless, undesirable interference caused by random body movement of an individual would still prevent us from obtaining the desired cardiac rate. This is because the maximum peak in the spectrum owing to the random body movement, except for both respiratory rate and its high-order harmonics often surpasses that of cardiac motion. To address this problem, we exploit the frequencies that appear most often in the histogram, which is the most innovative aspect in the proposed framework, compared with the conventional methods listed in [19]–[27].

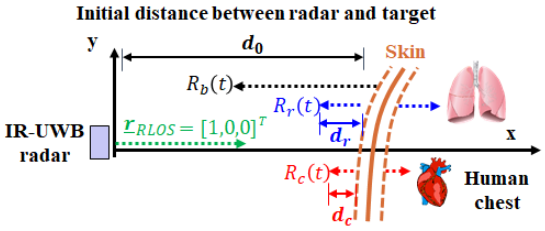

Fig. 1. Geometry of CRE for echo signal model.

The histogram requires a set of data samples [28]. For this, we need some phase frames with a frame time interval on a scale of milliseconds to gather many cardiac rate candidates. The three promising candidates for the desired cardiac rate can be selected as three frequencies corresponding to the 1st, 2nd, and 3rd maximum peaks in the histogram, which are values that appear most often in a set of data samples. This process is carried out under the assumption that the desired cardiac rates for each frame slowly fluctuate over a short time interval on the scale of milliseconds. To determine the desired cardiac rate from the three promising ones, we suggest a fuzzy rule-based method, which is an effective tool to provide human-like knowledge that comprises a group of fuzzy IF–THEN rules [29]–[30]. As a result, the desired cardiac rate can be successfully estimated via the proposed framework despite the low SNR caused by random body movement of an individual. The experimental results using a 7.29 GHz IR-UWB radar sensor and smartwatch show that our proposed scheme is capable of providing more accurate and robust real-time CRE performance compared to conventional methods.

This remainder of our paper is organized as follows: Section II introduces an echo signal model for CRE and discusses the difficulties in terms of CRE using measurements in the presence of body movement. Section III describes the proposed real-time CRE framework in detail. Section IV provides some experimental results to verify the proposed scheme. Finally, Section V presents our conclusions.

II. Echo Signal Model and Discussion

A. Echo Signal Model

In this section, we introduce an echo signal model to perform the CRE of an individual. The geometry of the

CRE for the echo signal model is shown in Fig. 1, where $\underline{\boldsymbol{r}}_{RLOS} = [1, 0, 0]^T$ is a radar line-of-sight (RLOS) vector. The range variation $R_r(t)$ along the radial direction for body's skin motion $\underline{\boldsymbol{r}}_r(t) = [d_r \cos(2\pi f_r(t)t + \varphi_{r_0}), 0, 0]^T$ caused by respiratory rate can be expressed as

$$R_r(t) = \underline{\boldsymbol{r}}_{RLOS}^T \cdot \underline{\boldsymbol{r}}_r(t) = d_r \cos(2\pi f_r(t)t + \varphi_{r_0}), \quad (1)$$

where $\cdot$ is the inner product operator, d_r is the variation of the range caused by the respiration motion, φ_{r_0} is the initial phase, and

$$f_r(t) = f_{r_0} + \Delta f_r \cos(2\pi f_{r_0} t) \quad (2)$$

is a real-time respiration rate function. Here, f_{r_0} is a fundamental frequency for respiration rate and, $\Delta f_r \cos(2\pi f_{r_0} t)$ is the slight variation in the respiration rate, leading to high-order harmonics in the spectrum of (1) due to the nonlinear relation between the input and output in the fast Fourier transform (FFT) process.

Next, the range variation $R_c(t)$ along the radial direction for the body's skin motion $\underline{\boldsymbol{r}}_c(t) = [d_c \cos(2\pi f_c(t)t + \varphi_{c_0}), 0, 0]^T$ caused by the cardiac rate can be represented as

$$R_c(t) = \underline{\boldsymbol{r}}_{RLOS}^T \cdot \underline{\boldsymbol{r}}_c(t) = d_c \cos(2\pi f_c(t)t + \varphi_{c_0}), \quad (3)$$

where d_c is the variation in the range caused by the cardiac motion, φ_{c_0} is the initial phase, and

$$f_c(t) = f_{c_0} + \Delta f_c \cos(2\pi f_{c_0} t) \quad (4)$$

is a real-time cardiac rate function. Here, f_{c_0} is the fundamental frequency for cardiac rate and $\Delta f_c \cos(2\pi f_{c_0} t)$ is the slight variation in the cardiac rate.

For an undesirable and simple body movement model, we assume that the range variation $R_b(t)$ along the radial direction for one-dimensional (1D) body movement $\underline{\boldsymbol{r}}_b(t) = [d_x(t), 0, 0]^T$ is expressed as follows:

$$R_b(t) = \underline{\boldsymbol{r}}_{RLOS}^T \cdot \underline{\boldsymbol{r}}_b(t) = d_x(t), \quad (5)$$

where $d_x(t)$ is the nonlinear variation of the range caused by the undesirable body movement of an individual.

For an IR-UWB echo signal model of an individual, a single radar-received pulse with a center frequency f_c and bandwidth BW (e.g., ultra-wideband $= f_c \pm BW/2 = 6.54 \sim 8.04$ GHz) is collected at the fast time t_{fast} after digitization using an analog-to-digital converter as follows:

$$s(t_{fast}) = I(t_{fast}) + j\,Q(t_{fast}), \quad (6)$$

where $I(t_{fast})$ and $Q(t_{fast})$ are the in-phase and quadrature signals, respectively. Subsequently, a sequential series of radar-received pulses is exploited to form a two-dimensional (2D) raw data frame $s(t_{fast}, t)$, where the slow time t is sampled by a pulse repetition frequency (PRF) f_{PRF} during a frame time T_F (i.e., $0 \le t \le T_F$, $\Delta t = 1/f_{PRF}$). Next, the matched-filtering in [31] is applied to the 2D raw data frame $s(t_{fast}, t)$ along the fast time t_{fast} to improve the SNR of the received signal:

$$\begin{aligned} s(R,t) &= \mathrm{MF}\{s(t_{fast},t)\}(0 \le R \le R_{max}, \Delta R = c/(2BW)), \\ &= I(R,t) + jQ(R,t), \end{aligned} \quad (7)$$

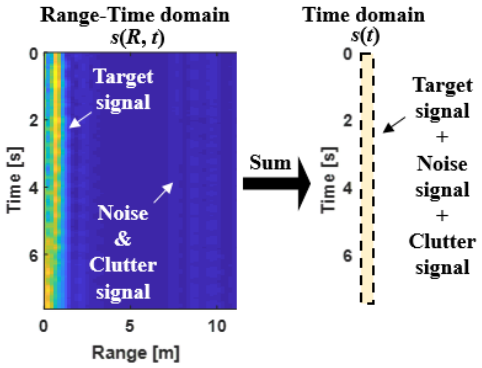

Fig. 2. Procedure to obtain the 1D IR-UWB echo signal model *s(t)* from 2D raw data frame *s(R, t)* of IR-UWB radar.

where MF{ } is the matched-filtering operator in [31], c is the speed of light, and R_{max} is the maximum range. We assume that an echo signal of an individual is returned from an ideal point scatter of the human chest engaged in the micromotions, as shown in (1), (3), and (5), and target's location is unknown in the range direction due to range migration effect caused by undesirable body movement of an individual. Then, an 1D IR-UWB echo signal $s(t)$ can be obtained by a sum of the raw data frame $s(R, t)$ in (7) along the range direction (see Fig. 2), as follows:

$$\begin{aligned} s(t) &= \sum_R s(R,t), \\ &= I(t) + jQ(t), \\ &= A(t)exp[j\theta(t)] + n(t) + n_c(t), \\ &= A(t)exp[\{j4\pi/\lambda_0\}\{d_0 + R_r(t) + R_c(t) + R_b(t)\}] \\ &\quad + n(t) + n_c(t), \end{aligned} \quad (8)$$

where λ_0 is the wavelength (i.e., $\lambda_0 = c/f_c$), A(t) is the magnitude information of the echo signal, $\theta(t)$ is the phase information of the echo signal, $n(t) = |n(t)|\angle\theta_{noise}(t)$ is the system noise, $n_c(t) = |n_c(t)|\angle\theta_{clutter}(t)$ is the background clutter, and d_0 is the initial distance between the radar and the human chest.

For CRE, we should obtain a fundamental frequency f_{c_0} in (4) from (8). To achieve this purpose, despite a nonlinear relationship among each phase term, the phase $\theta(t)$ in the echo signal $s(t)$ in (8) can be approximately extracted by applying an arctangent demodulation [4] to (8) as

$$\begin{aligned} \theta(t) &= \arctan\{Q(t)/I(t)\}, \\ &\approx \{4\pi/\lambda_0\}\{d_0 + R_r(t) + R_c(t) + R_b(t)\} \\ &\quad + \theta_{noise}(t) + \theta_{clutter}(t), \\ &\approx \theta_0 + \theta_r(t) + \theta_c(t) + \theta_b(t) + \theta_{noise}(t) + \theta_{clutter}(t), \end{aligned} \quad (9)$$

where θ_0, $\theta_r(t)$, $\theta_c(t)$, $\theta_b(t)$, $\theta_{noise}(t)$,and $\theta_{clutter}(t)$ are the phases of the initial distance, respiration rate, cardiac rate, undesirable body movement of an individual, system noise, and background clutter, respectively. Finally, CRE can be achieved by estimating the fundamental frequency f_{c_0} of the spectrum for phase $\theta_c(t)$ in (9). However, (9) has two problems in the real-time CRE: 1) phase ambiguity caused

by range variations more than half-wavelength, and 2) phase interference caused by a linear mixture of phases for the cardiac rate and undesirable components in (9), resulting in substantially lower SNR in terms of CRE. In Section IIB, these problems are discussed in detail.

B. Difficulties in CRE

To formulate the phase ambiguity problem caused only by the vital sign of an individual, we assume the ambiguity condition using (9) in special case (i.e., $\theta(t) \approx \theta_r(t) + \theta_c(t)$) as

$$|\theta_r(t) + \theta_c(t)| = |\{4\pi/\lambda_0\}\{R_r(t) + R_c(t)\}| > \pi/2. \quad (10)$$

When the wavelength λ_0 is short, the phase ambiguity in (10) may be caused by the vital sign. In addition, the maximum value of $R_r(t)$ (e.g., $0.001 \leq d_r \leq 0.003\ m$) is generally larger than that of $R_c(t)$ (e.g., $0.00005 \leq d_c \leq 0.0005\ m$); therefore, phase ambiguity is mostly dependent on the small range variance d_r in (1), not d_c in (3), leading to $|\theta_r(t) + \theta_c(t)| \approx 4\pi d_r/\lambda_0 > \pi/2$. Assuming that $d_r = 0.003\ m$, the criterion of λ_0 for the phase ambiguity caused by the respiration rate can be approximately expressed as

$$\lambda_0 < 8d_r < 0.024m. \quad (11)$$

Consequently, to prevent the phase ambiguity caused by the vital sign, λ_0 should be larger than approximately $0.024\ m$, resulting in a center frequency of $f_0 < 12.5$ GHz. Of course, the phase-unwrapping approaches in [17]–[18] can be used to increase the maximum range of f_0, but the phase ambiguity is still caused by the critical body movement of an individual in (5) due to $R_b(t) \gg R_r(t)$ in general.

Next, the phase interference causes significant trouble for CRE because the phase of a received echo signal is a linear mixture of a phase $\theta_c(t)$ for the cardiac rate and undesirable phases such as $\theta_r(t)$, $\theta_b(t)$, $\theta_{noise}(t)$, and $\theta_{clutter}(t)$ in (9). Therefore, we should solve the phase interference in an efficient manner for a robust and accurate CRE. For this, one of the widely used methods is band-pass filtering to remove undesirable phases [15]. However because high-order harmonics (e.g., $2f_{r_0}$, $3f_{r_0}$, and $4f_{r_0}$) of the respiration rate f_{r_0} usually exist in the frequency range (i.e., $0.83 \leq f_{c_0} \leq 1.83$ Hz) for cardiac rate f_{c_0}, CRE using only a band-pass filter may fail, especially in the presence of a body movement of an individual due to low SNR. On the contrary, another attractive alternative is to decompose the phase in (9) into two phases for the cardiac rate and undesirable terms. Recently, well-known signal decomposition methods such as EMD [26] and VMD [27] have been exploited to solve phase interference. However, when these methods [26]–[27] are adopted for real-time CRE in the presence of a body movement of an individual, the accuracy of CRE may not be guaranteed. This is because the body's skin motion for cardiac activity may be shaded or the RLOS may be rapidly changed by undesirable body's motion such as leaning forward and backward, leading to rapid degradation of SNR in terms of CRE. To intuitively demonstrate this problem, a measured echo signal using a 7.29 GHz IR-UWB radar is shown in Fig. 3(a) and the actual cardiac rate using a commercial smartwatch in Fig. 3(b). The experimental parameters are listed in Table I.

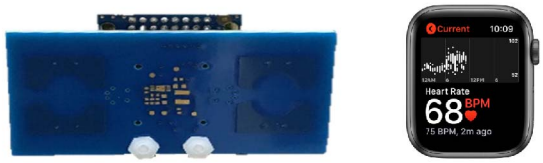

(a) (b)

Fig. 3. Measurement setup. (a) 7.29-GHz IR-UWB radar. (b) Smart watch.

TABLE I
EXPERIMENT PARAMETERS

Center frequency (f_c)	7.29 GHz
Wavelength (λ_0)	0.0412 m
Bandwidth (BW)	1.5 GHz
Maximum range (R_{max})	10 m
Frame time (T_F)	41.7 s
Pulse repetition frequency (f_{PRF})	24 Hz
Sample number of a phase frame (N_F)	1,000
Frame time interval (ΔT_F)	0.0417 s
Number of total phase frames (M)	2,000
Observation time (T_0)	125.02 s
Number of phase frames for histogram (L)	300
Initial distance (d_0)	0.2 m
False alarm rate (FAR)	0.2
Thresholding value (ξ_{th})	3 Hz
Upper bound of fuzzy variable 'slow' (th_1)	0.2
Lower bound of fuzzy variable 'fast' (th_2)	0.8

Fig. 4 presents the unwrapped phase and its spectrum for the measured echo signal in two scenarios: 1) a man sitting motionless in Fig. 4(a) and 2) a man slightly leaning forward in Fig. 4(d). In both scenarios, the phase ambiguity problem does not occur because the wavelength $\lambda_0 = 0.0412\ m$ of IR-UWB radar is not only larger than the criterion of $0.024\ m$ in (11), but the phase-unwrapping approach in [17]–[18] was also adopted (Fig. 4(b) and (e)). However, high-order harmonics such as $2f_{r_0}$, $3f_{r_0}$, and $4f_{r_0}$ of the respiration rate can be seen in the spectrum of the unwrapped phase using FFT (Fig. 4(c)). In particular, when the body of an individual leaned forward during $25 \leq t \leq 35\ s$, the unwrapped phase was rapidly distorted (Fig. 4(e)), leading to a significantly lowered peak for CRE, as shown in Fig. 4(f). Here, this lowered peak means that the cardiac rate f_{c_0} can no longer be estimated from the spectrum via conventional methods in [19]–[27] due to decreased SNR caused by the critical body movement of an individual.

For a more accurate and robust real-time CRE using the 7.29 GHz IR-UWB radar, we need to devise a new framework to address the phase interference problem discussed here. In Section III, the overall framework to solve this problem is explained in detail.

III. PROPOSED FRAMEWORK

In this section, we introduce the overall procedures for accurate and robust real-time CRE in the presence of a body

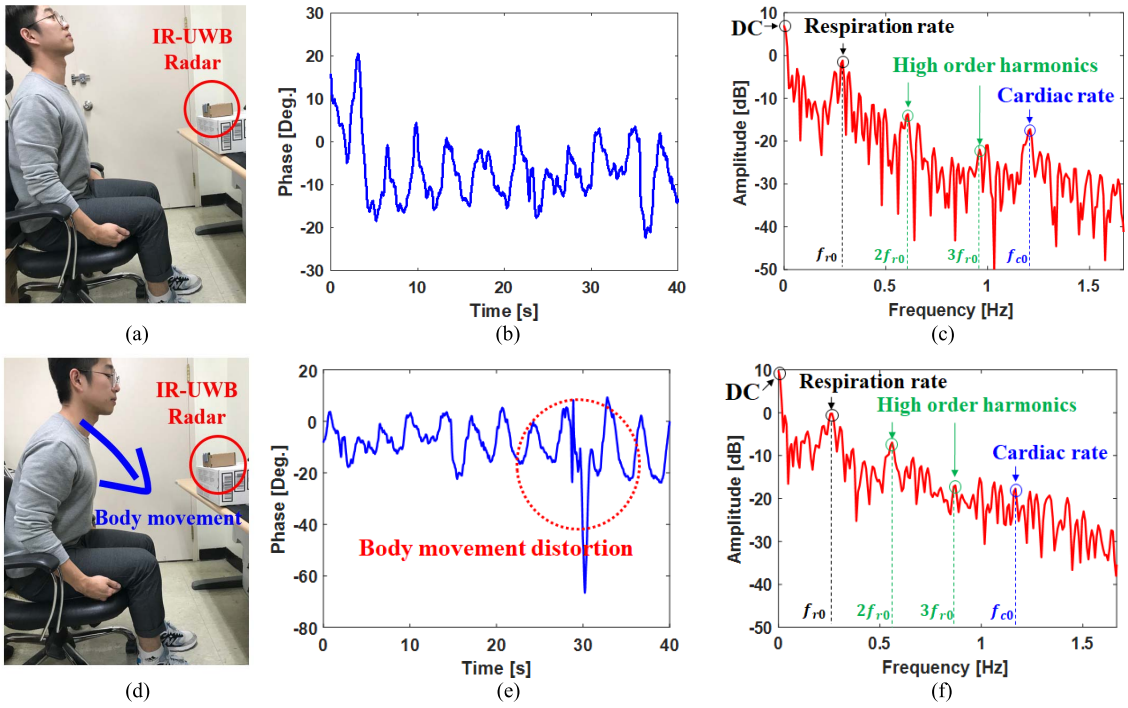

Fig. 4. Measurements using 7.29-GHz IR-UWB radar. (a) Scenario 1: a man sitting motionless. (b) Unwrapped phase of an echo signal received from (a). (c) Spectrum of (b). (d) Scenario 2: a man leaning forward. (e) Unwrapped phase of an echo signal received from (d). (f) Spectrum of (e).

movement of an individual. First, RRE via differentiation and spectrum analysis for an unwrapped phase is briefly introduced in Section IIIA. Second, the coarse estimation of cardiac rate candidates by excluding the respiratory rate and its high-order harmonics is discussed in Section IIIB. Third, the selection of three promising candidates for the desired cardiac rate based on frequencies that appear most often in the histogram is carried out in Section IIIC. Finally, a fuzzy logic rule-based method to determine the desired cardiac rate from three promising ones is suggested in Section IIID.

A. Respiratory Rate Estimation

For the proposed real-time CRE framework, we assume that M phase frames starting at frame time T_F are selected with the frame time interval ΔT_F on a scale of milliseconds during the observation time $T_0 = T_F + (M-1)\Delta T_F$ (Fig. 5). First, when the m^{th} unwrapped phase frame using the approach in [17]–[18] is selected for real-time CRE, we should estimate the respiratory rate f_{r0} in (2) to remove the effect of interference caused by the respiratory rate and its high-order harmonics.

Generally, the respiratory rate in the spectrum of the m^{th} unwrapped phase frame; $\theta_m(t)$ in (9) has the maximum peak only after we remove the frequency of DC around zero originating from background clutter (Fig. 4(c) and (f)). Subsequently, to perform RRE, we applied the differentiation to the m^{th} unwrapped phase $\theta_m(t)$ as follows:

$$\dot{\theta}_m(t) = \frac{d\theta_m(t)}{dt}. \tag{12}$$

According to [15], the respiratory rate f_{r0} can be estimated by selecting the frequency of a maximum peak in the spectrum

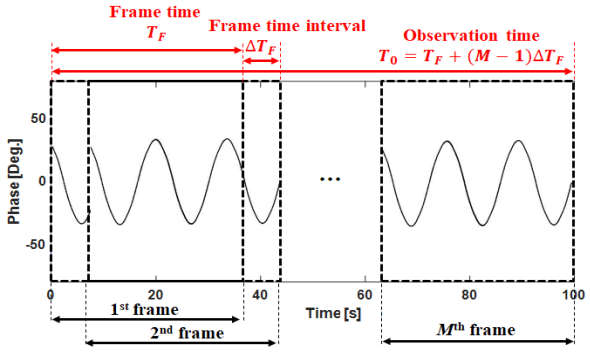

Fig. 5. M phase frames with frame time interval ΔT_F on the scale of milliseconds during observation time T_0.

of the unwrapped and differentiated phase in (12) as follows:

$$\hat{f}_{r0} = \arg \max_{0 < f < f_s/2} \left| FFT\{\dot{\theta}_m(t)\} \right|, \tag{13}$$

where $FFT\{\cdot\}$ is the FFT operator and f_s is the sampling frequency which is equal to the PRF f_{PRF} of the IR-UWB radar. In addition, we can predict the high-order harmonics, such as $2f_{r0}$, $3f_{r0}$, and $4f_{r0}$, by using the estimated respiratory rate from (13) because they are integer multiples of the estimated respiratory rate.

B. Coarse Estimation of Cardiac Rate Candidates

To coarsely estimate the cardiac rate candidates, the 1D cell averaging-constant false alarm rate (CA-CFAR) detector in [32] is applied to the spectrum of the m^{th} unwrapped and differentiated phase frame in (12). The false alarm rate for

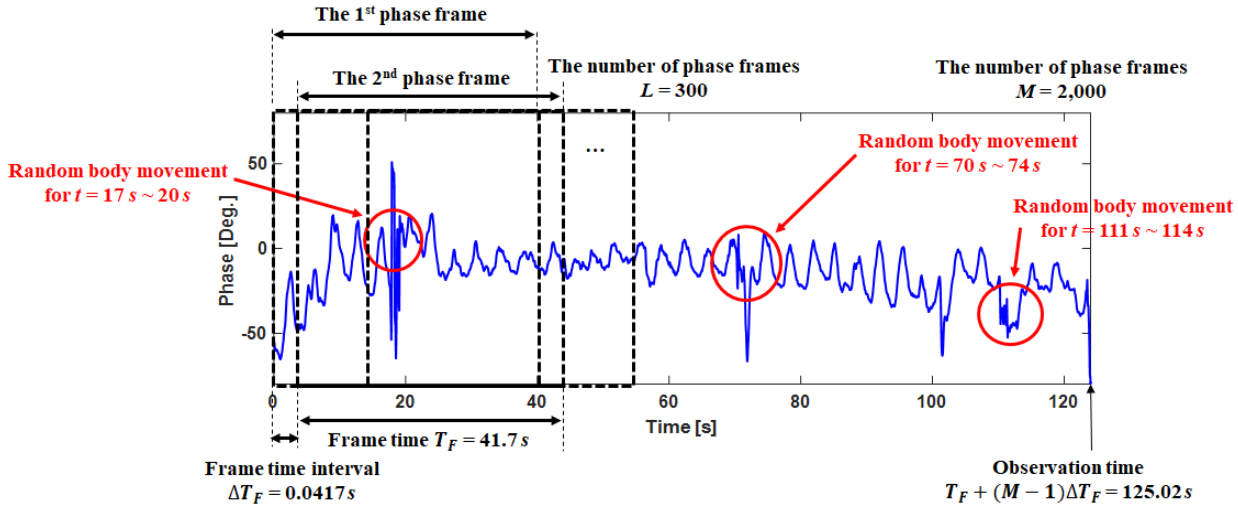

Fig. 6. Example of unwrapped phase frames of a measured echo signal for an observation time of 125.02 *s* for proposed real-time CRE framework.

the 1D CA-CFAR detector must be small enough to detect the cardiac rate candidates smaller than the strong phase noise caused by the critical random body movement of an individual (Fig. 4(f)).

Assuming that the jth frequency detected by 1D CA-CFAR for the m^{th} phase frame is c_j, $j = 1, \ldots, N_c$, where N_c is the number of detected frequencies, the respiratory rate and its high-order harmonics can be eliminated by comparing integer multiples of estimated respiratory rate in (13) as follows:

$$q_j = \begin{cases} 1, & \left| c_j - 1\hat{f}_{r0} \right| < \zeta_{th} \\ 2, & \left| c_j - 2\hat{f}_{r0} \right| < \zeta_{th} \\ 3, & \left| c_j - 3\hat{f}_{r0} \right| < \zeta_{th} \\ 0, & otherwise \end{cases} \tag{14}$$

where ξ_{th} is the thresholding value and q_j is the class decision to which the jth result c_j belongs to, which can be stated as follows: the respiratory rate ($q_j = 1$), the second-order harmonic of the respiratory rate ($q_j = 2$), the third-order harmonic of respiratory rate ($q_j = 3$), and cardiac rate candidate ($q_j = 0$). As a result, the cardiac rate candidates for the m^{th} phase frame can be obtained as p_j, $j = 1, \ldots, N_p$ ($N_p < N_c$), where N_p is the number of cardiac rate candidates, by excluding the respiratory rate and its high-order harmonics. However, difficulties in real-time CRE still exist because the peak information in the spectrum is no longer utilized to determine the desired cardiac rate from cardiac rate candidates (Fig. 4(f)). To solve this problem, we exploit the frequencies that appear most often in the histogram, which is the most innovative aspect in the proposed framework, compared with the conventional methods in [19]–[27].

C. Selection of Three Promising Candidates

Even though the peak of the desired cardiac rate in the spectrum may be smaller than that of the strong phase noise caused by critical body movement of an individual, it is assumed that the desired cardiac rate for the m^{th} phase frame would be one out of three frequencies ($f_{1,m}$, $f_{2,m}$, and $f_{3,m}$) corresponding to the 1st, 2nd, and 3rd maximum peaks in N_p cardiac rate candidates (e.g., p_1, p_2, …, p_{Np}) described in Section IIIB. Here, if a few phase frames of L ($L < M$) are selected from the m^{th} phase frame to the $(m+L)^{\text{th}}$ phase frame with a frame time interval ΔT_F on a scale of milliseconds (Fig. 6), each sample of three frequencies $f_{1,m}$, $f_{2,m}$, and $f_{3,m}$ above can be represented as $L \times 1$ vectors (i.e., $\underline{\mathbf{F}}_1$, $\underline{\mathbf{F}}_2$, and $\underline{\mathbf{F}}_3$) as follows:

$$\begin{aligned} \underline{\mathbf{F}}_1 &= [f_{1,1}, f_{1,2}, \ldots, f_{1,m}, \ldots, f_{1,L}]^T, \\ \underline{\mathbf{F}}_2 &= [f_{2,1}, f_{2,2}, \ldots, f_{2,m}, \ldots, f_{2,L}]^T, \\ \underline{\mathbf{F}}_3 &= [f_{3,1}, f_{3,2}, \ldots, f_{3,m}, \ldots, f_{3,L}]^T. \end{aligned} \tag{15}$$

From (15), we can approximately analyze the distribution of numerical values for the three frequencies, $f_{1,m}$, $f_{2,m}$, and $f_{3,m}$, via the histogram with $3L$ degrees of freedom due to a sample number of $3L$. This implies that we can use additional information to estimate the desired cardiac rate.

Generally, the desired cardiac rate during a short time interval is relatively stationary because this rate would slowly fluctuate on a scale of seconds (e.g., $0.54 \leq 1/f_{c0} \leq 1.2$ *s*), unlike rapidly fluctuating random phase noise [14]–[22]. The value that appears most often in a set of all samples in (15) can be represented as the most stationary value (i.e., the desired cardiac rate). Therefore, the desired cardiac rate f_{e1} can be estimated by selecting a frequency corresponding to the maximum peak in the histogram as follows:

$$f_{e1} = \arg \max_{0 < f < f_s/2} Hist\left\{ \left[\underline{\mathbf{F}}_1 \; \underline{\mathbf{F}}_2 \; \underline{\mathbf{F}}_3 \right]^T \right\}, \tag{16}$$

where $Hist\{\cdot\}$ is the histogram operator. Unfortunately, the estimated cardiac rate in (16) may vary very quickly at some phase frames during the observation time. This is because a frequency (i.e., f_{e2} or f_{e3}) corresponding to the 2nd or 3rd maximum peak in the histogram, not f_{e1}, can often become the desired cardiac rate owing to the effect of interferences caused by the critical body movement of an individual.

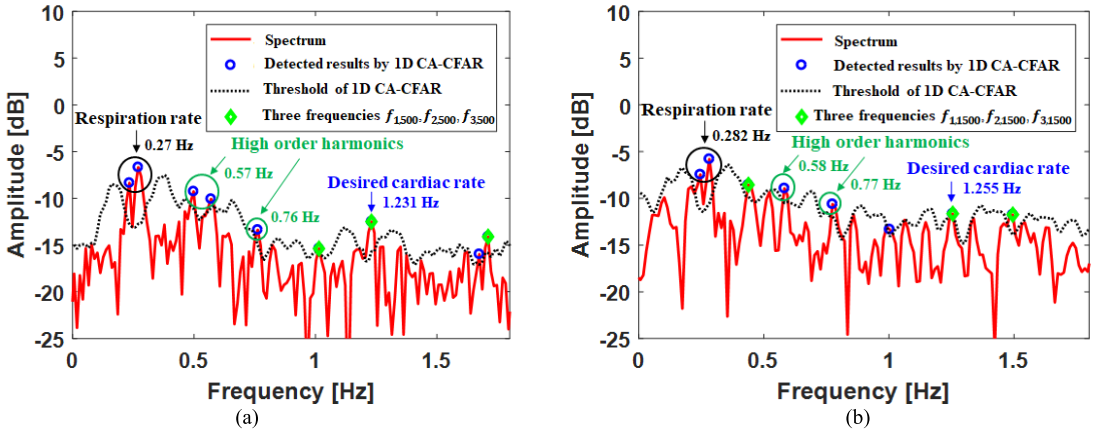

Fig. 7. Representation of the spectrums in two special cases (i.e., (a) and (b)). (a) The 500th unwrapped and differentiated phase frame at $t =$ 20.7917–62.4583 *s* in Fig. 6. (b) The 1500th unwrapped and differentiated phase frame at $t =$ 58.2917–99.9583 *s* in Fig. 6.

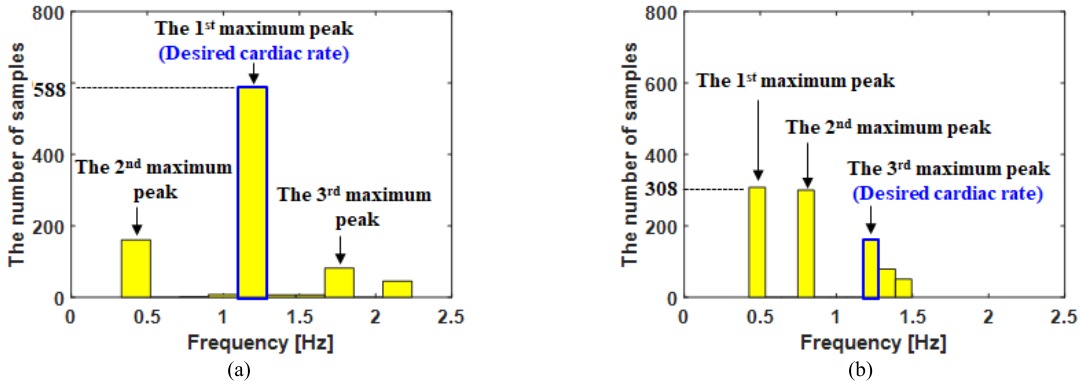

Fig. 8. Representation of the histograms in two special cases (i.e., (a) and (b)). (a) The histogram for many candidates obtained from phase frames of $L = 300$, including the result in Fig. 7(a). (b) The histogram for many candidates obtained from phase frames of $L = 300$, including the result in Fig. 7(b).

Consequently, this may cause a problem for the robustness of the proposed real-time CRE framework.

To show this problem, we utilized unwrapped phase frames of a measured echo signal during observation time 125.02 *s*, as shown in Fig. 6. The experimental parameters are the same as those presented in Section IIB. Fig. 7 shows an example of the spectrums in two special cases: 1) an unwrapped and differentiated phase frame of $m = 500$ at $t = 20.7917$–62.4583 *s* in Fig. 6, and 2) an unwrapped and differentiated phase frame of $m = 1500$ at $t = 58.2917$–99.9583 *s* in Fig. 6. Here, the information on cardiac rate contained in the spectrum shown in Fig. 7(b) was smeared and destroyed by body movement; thus, the desired cardiac rate was no longer determined as the maximum peak from three frequencies (i.e., $f_{1,1500}$, $f_{2,1500}$, and $f_{3,1500}$), unlike the results shown in Fig. 7(a).

Fig. 8 shows the experimental results of 2 histograms for many candidates obtained from phase frames of $L = 300$, including the results of the above-mentioned two special cases. A frequency corresponding to the maximum peak in the histogram shown in Fig. 8(a) is usually revealed as the desired cardiac rate, as shown in Fig. 7(a). However, when significant interference of body movement affects most phase frames for the histogram as shown in Fig. 7(b), the frequency corresponding to the maximum peak in the histogram was no longer the desired cardiac rate (Fig. 8(b)). Therefore, we should determine the desired cardiac rate from three promising candidates corresponding to the 1st, 2nd, and 3rd maximum peaks in the histogram in an efficient manner for robust real-time CRE.

For this purpose, we suggest a fuzzy rule-based method in Section IIID that contributes to the robustness of our proposed real-time CRE framework.

D. Fuzzy Rule-Based Real-Time CRE

Let us assume that three promising candidates $f_{e_1}(L+i)$, $f_{e_2}(L+i)$, and $f_{e_3}(L+i)$ corresponding to the 1st, 2nd, and 3rd maximum peaks in the histogram are selected at the $(L+i)^{th}$ phase frame. Subsequently, the real-time velocities (i.e., $v_{e_1}(i)$, $v_{e_2}(i)$, and $v_{e_3}(i)$, $i = 1, 2, \ldots, (M-L)$) between the $(L+i-1)^{th}$ phase frame and the $(L+i)^{th}$ phase frame can be represented as follows:

$$\begin{aligned} v_{e_1}(i) &= \{f_{e_1}(L+i) - f_{e_1}(L+i-1)\}/\Delta T_F, \\ v_{e_2}(i) &= \{f_{e_2}(L+i) - f_{e_1}(L+i-1)\}/\Delta T_F, \\ v_{e3}(i) &= \{f_{e_3}(L+i) - f_{e1}(L+i-1)\}/\Delta T_F, \end{aligned} \quad (17)$$

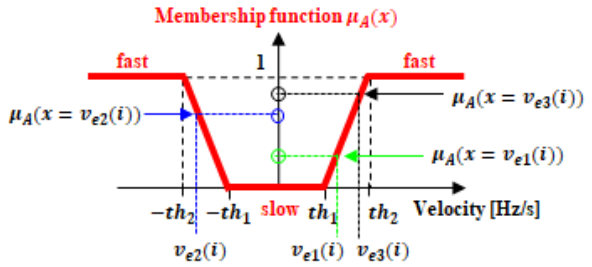

Fig. 9. Flowchart of the proposed real-time CRE framework in the presence of a body movement of an individual.

TABLE II
IF-THEN RULES FOR FUZZY LOGIC

	$\mu_A(v_{e1}(i)) < th_1$	$th_1 \le \mu_A(v_{e1}(i)) < th_2$	$th_2 \le \mu_A(v_{e1}(i))$
$\mu_A(v_{e2}(i)) < th_1$	$\hat{f}_{c0}(i) = f_{e1}(L+i)$	$\hat{f}_{c0}(i) = f_{e2}(L+i)$	$\hat{f}_{c0}(i) = f_{e2}(L+i)$
$th_1 \le \mu_A(v_{e2}(i)) < th_2$	$\hat{f}_{c0}(i) = f_{e1}(L+i)$	If $\mu_A(v_{e3}(i)) < th_1$, then $\hat{f}_{c0}(i) = f_{e3}(L+i)$ If $th_1 \le \mu_A(v_{e3}(i))$, then $\hat{f}_{c0}(i) = \hat{f}_{c0}(i-1)$	If $\mu_A(v_{e3}(i)) < th_1$, then $\hat{f}_{c0}(i) = f_{e3}(L+i)$ If $th_1 \le \mu_A(v_{e3}(i))$, then $\hat{f}_{c0}(i) = \hat{f}_{c0}(i-1)$
$th_2 \le \mu_A(v_{e2}(i))$	$\hat{f}_{c0}(i) = f_{e1}(L+i)$	If $\mu_A(v_{e3}(i)) < th_1$, then $\hat{f}_{c0}(i) = f_{e3}(L+i)$ If $th_1 \le \mu_A(v_{e3}(i))$, then $\hat{f}_{c0}(i) = \hat{f}_{c0}(i-1)$	If $\mu_A(v_{e3}(i)) < th_1$, then $\hat{f}_{c0}(i) = f_{e3}(L+i)$ If $th_1 \le \mu_A(v_{e3}(i))$, then $\hat{f}_{c0}(i) = \hat{f}_{c0}(i-1)$

where $f_{e_1}(L+i-1)$ is a promising candidate corresponding to the 1st maximum peak in the histogram at the $(L+i-1)^{\text{th}}$ phase frame. If $f_{e_1}(L+i-1)$ is the desired cardiac rate at the $(L+i-1)^{\text{th}}$ phase frame, the real-time velocity of the desired cardiac rate at the $(L+i)^{\text{th}}$ phase frame will be close to zero because the frame time interval ΔT_F is very short; thus, the real-time variation of the desired cardiac rate is significantly slow. Therefore, real-time velocities in (17) enable us to determine the desired cardiac rate from three promising ones. In this regard, the fuzzy logic rule-based method is a simple and effective tool that provides human-like knowledge that comprises a group of fuzzy IF–THEN rules [29]–[30].

We define the i^{th} fuzzy sets in $\boldsymbol{U}_i = \{v_{e_1}(i), v_{e_2}(i), v_{e_3}(i)\}$ to apply the fuzzy logic rule-based approach to the real-time CRE framework. Assuming that a fuzzy set is characterized by a membership function $\mu_{\boldsymbol{A}}(x)$ that takes values in the interval [0, 1] and an input x for the fuzzy system has three velocities in $\boldsymbol{U}_i$, the i^{th} fuzzy sets $\boldsymbol{A}$ can be defined as

$$\boldsymbol{A} = \{(x, \mu_{\boldsymbol{A}}(x)) | x \in \boldsymbol{U}_i\}, \tag{18}$$

where $\mu_{\boldsymbol{A}}(x)$ is defined as trapezoid-shaped curves to assign real-time velocities of three promising candidates to fuzzy sets with some degree of membership (see Fig. 9).

Next, the IF–THEN rules for fuzzy logic are defined as shown in Table II. Then, we execute all applicable rules in Table II to compute the output values. For example, given a certain velocity of $v_{e_1}(i)$, its membership function is smaller than the upper bound of fuzzy variable "slow" (i.e., th_1), which is copied to the output value that $\hat{f}_{c0}(i) = f_{e_1}(L+i)$. In contrast, if $\mu_{\boldsymbol{A}}(v_{e_1}(i))$ and $\mu_{\boldsymbol{A}}(v_{e_2}(i))$ have fuzzy variables "fast" and "slow" (i.e., $th_2 \le \mu_{\boldsymbol{A}}(v_{e_1}(i))$ and $\mu_{\boldsymbol{A}}(v_{e_2}(i)) < th_1$), the output value can be represented as $\hat{f}_{c0}(i) = f_{e_2}(L+i)$. However, when all values in the i^{th} fuzzy sets are larger than the lower bound of fuzzy variable 'fast' (i.e., th_2), the i^{th} output value is substituted for the $(i-1)^{\text{th}}$ output value.

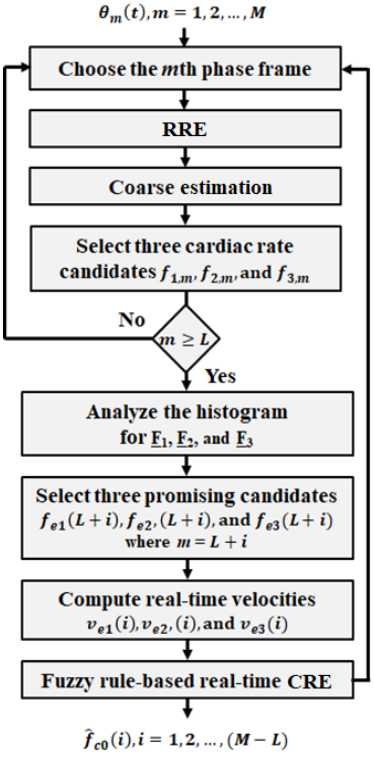

Fig. 10. Membership function for fuzzy logic-rule based real-time CRE.

In summary, the flowchart for the proposed real-time CRE framework is illustrated in Fig. 10. In the next section, we demonstrate the performance of the proposed scheme using measurements obtained by a 7.29 GHz IR-UWB radar sensor and smartwatch.

IV. EXPERIMENTAL RESULTS

To verify the performance of the proposed real-time CRE framework in the presence of a body movement via measurements, we used a 7.29 GHz IR-UWB radar sensor with a 1 GHz bandwidth (Fig. 3(a)). The individual was approximately 0.2 m away from the radar sensor, and its actual cardiac rate was measured by using a smart watch (see Fig. 3(b)), which is an assessment tool to verify the accuracy of the proposed real-time CRE. Subsequently, to obtain the unwrapped phase frames of $M = 2{,}000$ for real-time CRE, we measured an echo signal received from chest of a human with the frame time interval of $\Delta T_F = 0.0417$ s during the observation time $T_0 = 125.02$ s as shown in Fig. 4(a). Random body movements of an individual such as leaning forwards and backwards occur at $t = 17$–20 s, $t = 70$–74 s, and $t = 111$–114 s, respectively (Fig. 6).

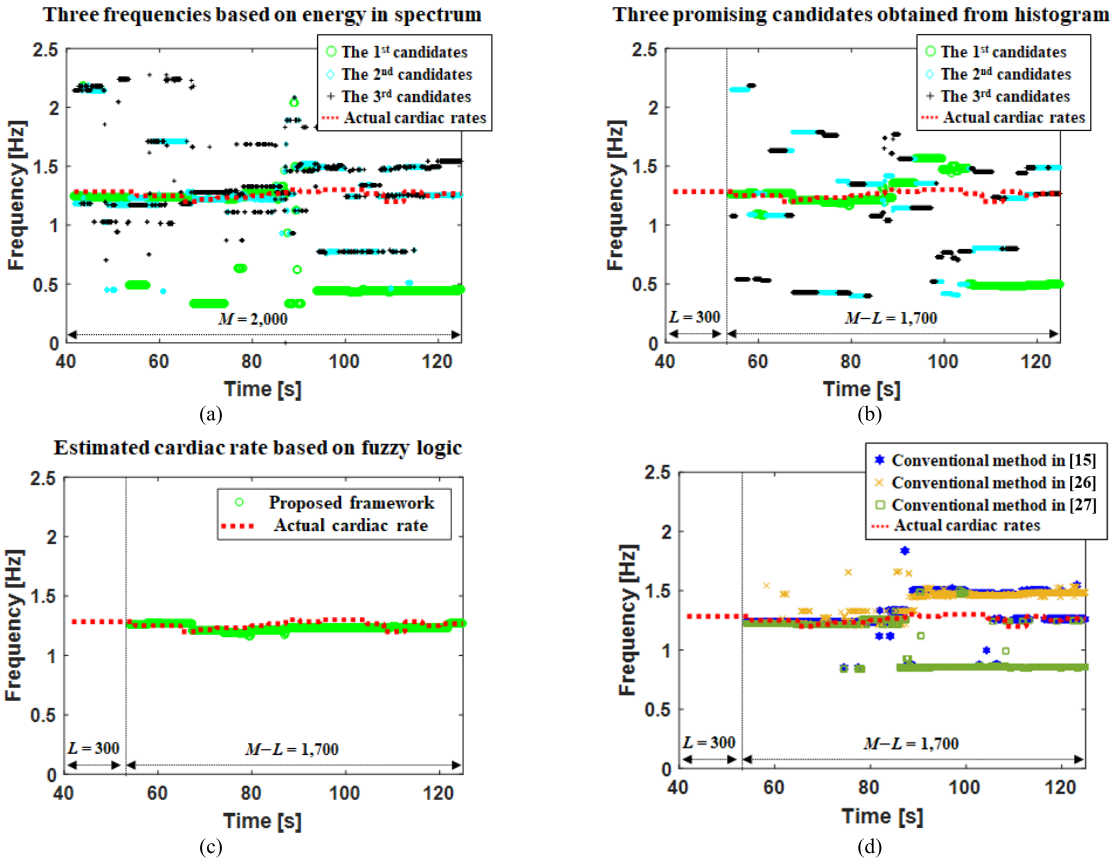

Fig. 11. Experimental results to investigate the CRE performance on the proposed framework (i.e., (a)–(c)) and conventional methods (i.e., (d)). (a) RRE + Coarse estimation. (b) RRE + Coarse estimation + Selection of three promising candidates. (c) RRE + Coarse estimation + Selection of three promising candidates + Fuzzy rule-based real-time CRE. (d) Conventional methods.

For RRE and CRE, spectrum analysis was conducted by applying FFT to unwrapped and differentiated phase with zero padding by a factor of 2, leading to the frequency resolution of 0.012 Hz. For the fuzzy system, the upper and lower bounds of the fuzzy variables are empirically selected as $th_1 = 0.2$ and $th_2 = 0.8$, respectively. The detailed parameters of this experiment are listed in Table I.

A. Robustness of Our Proposed Framework

To verify the robust CRE performance of the proposed framework, the experiments were performed in three cases: 1) RRE + coarse estimation shown in Fig. 11(a), 2) RRE + coarse estimation + selection of three promising candidates shown in Fig. 11(b), and 3) RRE + coarse estimation + selection of three promising candidates + fuzzy rule-based real-time CRE, as shown in Fig. 11(c).

Fig. 11(a) shows the 3 frequencies—$f_{1,m}$, $f_{2,m}$, and $f_{3,m}$—corresponding to the 1st, 2nd, and 3rd maximum peaks in the spectrum of the unwrapped and differentiated phase frames with $M = 2{,}000$ during the observation time via RRE + coarse estimation. Fig. 11(a) shows that a cardiac rate candidate corresponding to the 1st maximum peak exhibits a very similar actual cardiac rate to the smart watch, when $t = 41.7$–85 s. However, when $t = 85$–125.02 s, CRE based on the 1st maximum peak in the spectrum failed to estimate the desired cardiac rate due to the peak of strong phase noise caused by critical body movement of an individual larger than that of the desired cardiac rate.

Next, we analyzed the numerical distribution using 1,500 samples of 3 frequencies in Fig. 11(a) for phase frames of $L = 300$. After performing RRE + coarse estimation + selection of three promising candidates, three promising candidates (i.e., f_{e_1}, f_{e_2}, and f_{e_3}) corresponding to the 1st, 2nd, and 3rd maximum peaks in the histogram were extracted, as shown in Fig. 11(b). Here, even though additional information to estimate the desired cardiac rate was exploited for real-time CRE, the frequency corresponding to the 1st maximum peak in the histogram has some mismatch relative to the actual cardiac rate at $t = 85$–125 s in Fig. 11(b). This is because a frequency (i.e., f_{e_2} or f_{e_3}) corresponding to the 2nd or 3rd maximum peak in the histogram can be the desired cardiac rate owing to the effect of interference caused by the critical random body movement of an individual.

Finally, we estimated the desired cardiac rate by applying the fuzzy rule-based method to the real-time velocities of the three promising candidates in Fig. 11(b) (Fig. 11(c)). The estimated cardiac rate in Fig. 11(c) was significantly robust to the strong phase noise caused by critical body movement of an individual via fuzzy rule-based real-time CRE, unlike the two cases in Fig. 11(a)–(b). This is because real-time velocities for fuzzy logic enable us to determine the desired cardiac rate

TABLE III
COMPARISON OF RMSE OF ESTIMATED CARDIAC RATE BETWEEN CONVENTIONAL METHODS AND OUR PROPOSED METHOD

	RMSE for a male	RMSE for a female
Conventional method in [15]	0.1718	0.1691
Conventional method in [26]	0.1683	0.1410
Conventional method in [27]	0.2857	0.2033
Proposed method	0.0402	0.0357

from three promising candidates in the presence of a body movement of an individual.

For a quantitative comparison of the robustness between the proposed framework and conventional methods, we conducted additional experiments using representative conventional methods [15], [26], and [27] (Fig. 11(d)). Here, the conventional method in [15] selected a desired cardiac rate corresponding to the 1st maximum peak in the spectrum with band-pass filtering (e.g., $0.83 \leq f_{c0} \leq 1.83$ Hz) for the actual cardiac rate f_{c0}. Similarly, the other conventional methods in [26]–[27] utilized the same conventional method as in [15] for CRE, except for signal decomposition techniques such as EMD in [26] and VMD in [27]. In this experiment, the conventional methods in [15], [26], and [27] were very sensitive to the strong phase noise, especially at $t = 85$–125 s in Fig. 11(d) because these methods conduct the CRE based on the amplitude in the spectrum, unlike our proposed framework. These results lead us to conclude that our proposed real-time CRE framework is robust to strong phase noise caused by the critical random body movement of an individual in comparison with the conventional methods in [15], [26], and [27].

B. Estimation Accuracy

To quantitatively evaluate the accuracy of the proposed real-time CRE framework, we computed the root-mean-square error (RMSE) between the actual cardiac rate of the smartwatch and the estimated cardiac rate, which is defined as

$$RMSE = \sqrt{\frac{1}{M-L}\sum_{i=1}^{M-L}\left(f_{c0}(i) - \hat{f}_{c0}(i)\right)^2}, \qquad (19)$$

where $f_{c0}(i)$ and $\hat{f}_{c0}(i)$ denote the i^{th} actual cardiac rate and estimated cardiac rate, respectively. We compared the RMSE of our proposed method in Fig. 11(c) with those of the conventional methods [15], [26], and [27] in Fig. 11(d). In addition, to verify the effect of another individual on the proposed real-time CRE framework, we conducted additional experiments for a female by using the same parameters as those used for the CRE of a male in Fig. 4.

The results of two experiments to investigate the performance of the proposed framework are summarized in Table III. The performance attained in the two experiments are quite similar despite the different random body movements of an individual. These results verify that our proposed framework is robust to the targets. Moreover, to verify the effect of distance and orientation between the radar and the target, we conducted additional experiments under different distances, 2, 4, and 8 m and orientations, 15, 30, and 45° of an individual. Fig. 12(a) and (b) show the RMSEs of our proposed method and conventional methods [15], [26], and [27] for various distances and orientations, respectively. We can see that when the distance or the orientation between the radar and target increased, CRE performance gradually degraded due to decreased SNR. However, the cardiac rate estimated by our proposed framework was very accurate, compared with the conventional methods. From the above discussions, we can conclude that the proposed framework provides accurate and robust real-time CRE performance in the presence of body movement.

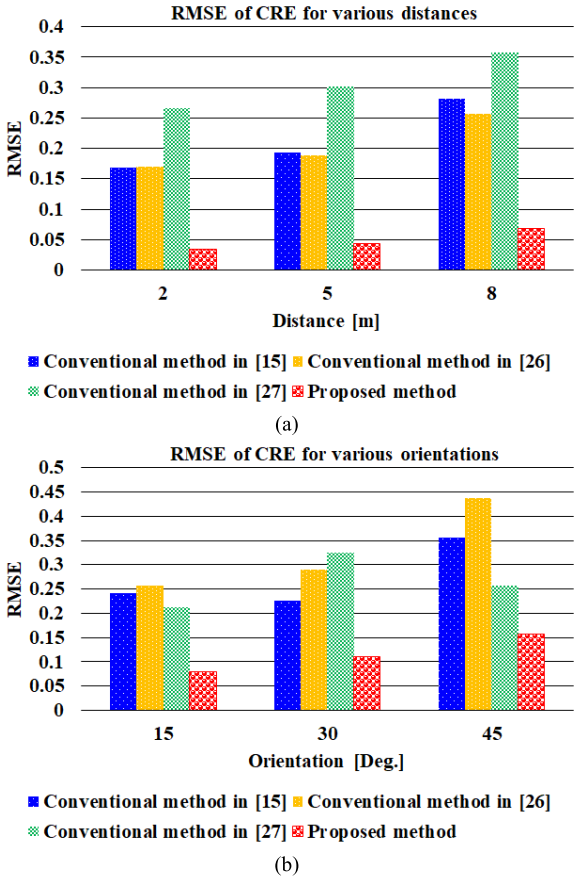

Fig. 12. Experimental results to investigate the effect of distance and orientation of an individual. (a) RMSE of CRE for various distances. (b) RMSE of CRE for various orientations.

C. Computational Efficiency

To verify the computational efficiency of the proposed real-time CRE framework, we compared the computational complexity of our proposed method with those of conventional methods in [15], [26], and [27], where MATLAB R2017a, which ran on a computer running Window 10 with an Intel i7 processor, was used for this experiment.

In this experiment, the computational time (i.e., 0.01133 s) of the proposed CRE framework for a single-phase frame was less than a frame time interval of $\Delta T_F = 0.0417$ s, whereas those of the two conventional methods in [26] and [27] were

TABLE IV
COMPARISON OF COMPUTATION TIME OF ESTIMATED CARDIAC RATE BETWEEN CONVENTIONAL METHODS AND PROPOSED METHOD

	Computation time [s]
Conventional method in [15]	0.00026
Conventional method in [26]	0.14618
Conventional method in [27]	0.07903
Proposed method	0.01133

more than 0.0417 s owing to the interpolation step and iterative optimization algorithm, respectively (see Table IV). This implies that our proposed method can achieve real-time CRE processing within a frame time interval with good performance in terms of both accuracy and robustness, compared to the conventional methods in [15], [26], and [27].

V. CONCLUSION

In this paper, a new framework for real-time CRE in the presence of body movement was introduced. Our proposed scheme was performed in four steps: (i) RRE via differentiation and spectrum analysis for the unwrapped phase; (ii) coarse estimation of cardiac rate candidates by excluding the respiratory rate and its high-order harmonics; (iii) selecting three promising candidates based on frequencies that appear most often in the histogram for several candidates; and (iv) determination of the desired cardiac rate from three promising candidates via a fuzzy logic rule-based method. In the experiment using a 7.29 GHz IR-UWB radar sensor and smartwatch, we observed that our proposed framework was capable of performing more accurate and robust real-time CRE in the presence of a body movement of an individual compared with conventional methods.

Future work will involve a study of the translational motion compensation techniques for real-time CRE of a human under a simple walking motion instead of small body movement. This is because the walking motion causes three critical problems in real-time CRE: i) phase ambiguity caused by walking motion, ii) phase interference caused by multiple scatterers on certain body parts (e.g., arms and legs) with undesirable micromotions, and iii) the range-migration effect.

REFERENCES

[1] E. M. Staderini, "UWB radars in medicine," *IEEE Aerosp. Electron. Syst. Mag.*, vol. 17, no. 1, pp. 13–18, Jan. 2002.

[2] A. D. Droitcour *et al.*, "Range correlation and I/Q performance benefits in single-chip silicon Doppler radar for noncontact cardiopulmonary monitoring," *IEEE Trans. Microw. Theory Techn.*, vol. 52, no. 3, pp. 838–848, Mar. 2004.

[3] C. Gu *et al.*, "Accurate respiration measurement using DC-coupled continuous-wave radar sensor for motion-adaptive cancer radiotherapy," *IEEE Trans. Biomed. Eng.*, vol. 59, no. 11, pp. 3117–3123, Nov. 2012.

[4] W. Hu, Z. Zhao, Y. Wang, H. Zhang, and F. Lin, "Noncontact accurate measurement of cardiopulmonary activity using a compact quadrature Doppler radar sensor," *IEEE Trans. Biomed. Eng.*, vol. 61, no. 3, pp. 725–735, Mar. 2014.

[5] Y.-J. An, G.-H. Yun, and J.-G. Yook, "Sensitivity enhanced vital sign detection based on antenna reflection coefficient variation," *IEEE Trans. Biomed. Circuits Syst.*, vol. 10, no. 2, pp. 319–327, Apr. 2016.

[6] C. Li *et al.*, "A review on recent progress of portable short-range noncontact microwave radar systems," *IEEE Trans. Microw. Theory Techn.*, vol. 65, no. 5, pp. 1692–1706, May 2017.

[7] J.-K. Park *et al.*, "Noncontact RF vital sign sensor for continuous monitoring of driver status," *IEEE Trans. Biomed. Circuits Syst.*, vol. 13, no. 3, pp. 493–502, Jun. 2019.

[8] Y. Zhang, F. Qi, H. Lv, F. Liang, and J. Wang, "Bioradar technology: Recent research and advancements," *IEEE Microw. Mag.*, vol. 20, no. 8, pp. 58–73, Aug. 2019.

[9] H. Lee, B.-H. Kim, J.-K. Park, S. W. Kim, and J.-G. Yook, "A resolution enhancement technique for remote monitoring of the vital signs of multiple subjects using a 24 GHz bandwidth-limited FMCW radar," *IEEE Access*, vol. 8, pp. 1240–1248, Dec. 2020.

[10] A. Lazaro, D. Girbau, and R. Villarino, "Analysis og vital signs monitoring using AN IR-UWB radar," *Prog. Electromagn. Res.*, vol. 100, pp. 265–284, 2010.

[11] A. Nezirovic, A. G. Yarovoy, and L. P. Ligthart, "Signal processing for improved detection of trapped victims using UWB radar," *IEEE Trans. Geosci. Remote Sens.*, vol. 48, no. 4, pp. 2005–2014, Apr. 2010.

[12] J. Sachs, *Handbook of Ultra-Wideband Short-Range Sensing: Theory Sensors Applications*. Hoboken, NJ, USA: Wiley, 2013.

[13] A. Lazaro, D. Girbau, and R. Villarino, "Techniques for clutter suppression in the presence of body movements during the detection of respiratory activity through UWB radars," *Sensors*, vol. 14, no. 2, pp. 2595–2618, Feb. 2014.

[14] J. Sachs and R. Herrmann, "M-sequence-based ultra-wideband sensor network for vitality monitoring of elders at home," *IET Radar, Sonar Navigat.*, vol. 9, no. 2, pp. 125–137, Feb. 2015.

[15] F. Adib, H. Mao, Z. Kabelac, D. Katabi, and R. C. Miller, "Smart homes that monitor breathing and heart rate," in *Proc. 33rd Annu. ACM Conf. Hum. Factors Comput. Syst.*, Apr. 2015, pp. 837–846.

[16] I. V. Mikhelson, S. Bakhtiari, T. W. Elmer, and A. V. Sahakian, "Remote sensing of heart rate and patterns of respiration on a stationary subject using 94-GHz millimeter-wave interferometry," *IEEE Trans. Biomed. Eng.*, vol. 58, no. 6, pp. 1671–1677, Jun. 2011.

[17] S. Kim and C. Nguyen, "On the development of a multifunction millimeter-wave sensor for displacement sensing and low-velocity measurement," *IEEE Trans. Microw. Theory Techn.*, vol. 52, no. 11, pp. 2503–2512, Nov. 2004.

[18] Q. Lv *et al.*, "High dynamic-range motion imaging based on linearized Doppler radar sensor," *IEEE Trans. Microw. Theory Techn.*, vol. 62, no. 9, pp. 1837–1846, Sep. 2014.

[19] J. Tu, T. Hwang, and J. Lin, "Respiration rate measurement under 1-D body motion using single continuous-wave Doppler radar vital sign detection system," *IEEE Trans. Microw. Theory Techn.*, vol. 64, no. 6, pp. 1937–1946, Jun. 2016.

[20] C. Li and J. Lin, "Random body movement cancellation in Doppler radar vital sign detection," *IEEE Trans. Microw. Theory Techn.*, vol. 56, no. 12, pp. 3143–3152, Dec. 2008.

[21] E. Schires, P. Georgiou, and T. S. Lande, "Vital sign monitoring through the back using an UWB impulse radar with body coupled antennas," *IEEE Trans. Biomed. Circuits Syst.*, vol. 12, no. 2, pp. 292–302, Apr. 2018.

[22] T.-H. Liu, M.-L. Hsu, and Z.-M. Tsai, "High ranging accuracy and wide detection range interferometry based on frequency-sweeping technique with vital sign sensing function," *IEEE Trans. Microw. Theory Techn.*, vol. 66, no. 9, pp. 4242–4251, Sep. 2018.

[23] C. Gu, Z. Peng, and C. Li, "High-precision motion detection using low-complexity Doppler radar with digital post-distortion technique," *IEEE Trans. Microw. Theory Techn.*, vol. 64, no. 3, pp. 961–971, Mar. 2016.

[24] E. Yavari and O. Boric-Lubecke, "Channel imbalance effects and compensation for Doppler radar physiological measurements," *IEEE Trans. Microw. Theory Techn.*, vol. 63, no. 11, pp. 3834–3842, Nov. 2015.

[25] M. He, Y. Nian, and B. Liu, "Noncontact heart beat signal extraction based on wavelet transform," in *Proc. 8th Int. Conf. Biomed. Eng. Informat. (BMEI)*, Oct. 2015, pp. 14–16.

[26] J. Feng and S. Pan, "Extraction algorithm of vital signals based on empirical mode decomposition," *J. South China Uni. Techn.*, vol. 38, pp. 1–6, Oct. 2010.

[27] C. Ding, J. Yan, L. Zhang, H. Zhao, H. Hong, and X. Zhu, "Noncontact multiple targets vital sign detection based on VMD algorithm," in *Proc. IEEE Radar Conf. (RadarConf)*, May 2017, pp. 8–12.

[28] S. Theodoridis, *Pattern Recognition*. New York, NY, USA: Academic, 2003.

[29] C. Garcia and M. Delakis, "Convolutional face finder: A neural architecture for fast and robust face detection," *IEEE Trans. Pattern Anal. Mach. Intell.*, vol. 26, no. 11, pp. 1408–1423, Nov. 2004.

[30] C. Quek, M. Pasquier, and B. B. Seng Lim, "POP-TRAFFIC: A novel fuzzy neural approach to road traffic analysis and prediction," *IEEE Trans. Intell. Transp. Syst.*, vol. 7, no. 2, pp. 133–146, Jun. 2006.

[31] J.-H. Choi, J.-E. Kim, and K.-T. Kim, "People counting using IR-UWB radar sensor in a wide area," *IEEE Internet Things J.*, early access, Oct. 21, 2020, doi: 10.1109/JIOT.2020.3032710.
[32] B. Mahuza, *MATLAB Simulations for Radar Systems Design Using MATLAB*. Boca Raton, FL, USA: CRC Press, 2000.

Inoh Choi received the B.S. and M.S. degrees in electronic engineering from Pukyong National University, Busan, South Korea, in 2012 and 2014, respectively, and the Ph.D. degree in electronic engineering from the Pohang University of Science and Technology (POSTECH), Pohang, South Korea, in 2020. From 2019 to 2021, he was a Senior Researcher with the Agency for Defense Development (ADD). In 2021, he joined the faculty of the Department of Electronics and Communications Engineering, Korea Maritime & Ocean University, Busan, where he is currently a Professor. His current research area of interests include micro-Doppler analysis, ballistic target discrimination, vital sign detection, automotive target recognition, and calibration of polarimetric SAR.

Min Kim received the B.S. and M.S. degrees in electronic engineering from Pukyong National University, Busan, South Korea, in 2015 and 2017, respectively. He is currently pursuing the Ph.D. degree in electronic engineering with the Pohang University of Science and Technology (POSTECH). His current research area of interests include radar target recognition and multitargets tracking.

Jaeho Choi received the B.S. degree in computer engineering from Korea University, Seoul, South Korea, in 2017, and the M.S. degree electronic engineering from the Pohang University of Science and Technology (POSTECH), Pohang, South Korea, in 2019, where he is currently pursuing the Ph.D. degree in the electronic engineering. His current research area of interests includes people counting and deep learning.

Jeongki Park received the B.S. and M.S. degrees in electronic engineering from the Pohang University of Science and Technology (POSTECH), Pohang, South Korea, in 2018 and 2020, respectively, where he is currently pursuing the Ph.D. degree in electronic engineering. His current research area of interests include vehicle radar signal processing and vital sign detection.

Sanghong Park received the B.S., M.S., and Ph.D. degrees in electronic engineering from the Pohang University of Science and Technology (POSTECH), Pohang, South Korea, in 2004, 2007, and 2010, respectively. In 2010, he was a Brain Korea 21 Postdoctoral Fellow with the Electromagnetic Technology Laboratory, POSTECH. In 2010, he joined the faculty of the Department of Electronics Engineering, Pukyong National University, Busan, South Korea, where he is currently a Professor. His research interests include the areas of radar target imaging and recognition, radar signal processing, target motion compensation, and radar cross section prediction.

Kyungtae Kim (Member, IEEE) received the B.S., M.S., and Ph.D. degrees from POSTECH, Pohang, South Korea, in 1994, 1996, and 1999, respectively, all in electrical engineering. From 2002 to 2010, he was a Faculty Member with the Department of Electronic Engineering, Yeungnam University. Since 2011, he has been with the Department of Electrical Engineering, POSTECH, where he is currently a Professor. From 2012 to 2017, he served as the Director for the Sensor Target Recognition Laboratory, sponsored by the Defense Acquisition Program Administration and the Agency for Defense Development. He is currently the Director of both the Next Generation Imaging Radar System Research Center, and the Next Generation Defense Multidisciplinary Technology Research Center at POSTECH. He is an author of about 300 articles on journals and conference proceedings. His research interests include the field of intelligent radar system and signal processing: SAR/inverse SAR imaging, target recognition, detection/estimation/tracking, radar resource management, direction of arrival estimation, micro-Doppler analysis, digital beamforming, electronic warfare, and indoor monitoring of individuals. He is a member of the KIEES. He is currently carrying out several research projects funded by the Korean Government and several industries. He was a recipient of several outstanding research awards and best paper awards from the Korea Institute of Electromagnetic Engineering and Science (KIEES), and international conferences.